

Article

Synthesis and Crystal Structures of Mn(II) and Co(II) Complexes as Catalysts for Oxidation of Cyclohexanone

Adedibu C. Tella^{1,2,*}, Aaron Y. Isaac^{1,3}, Hadley S. Clayton², Adeniyi S. Ogunlaja⁴ , Aswathy T. Venugopalan^{3,5}, Marimuthu Prabu^{3,5} and Raja Thirumalaiswamy^{3,5}¹ Department of Chemistry, University of Ilorin, P.M.B. 1515, Ilorin 240003, Nigeria; aaryone1@gmail.com² Department of Chemistry, University of South Africa, Unisa 0003, South Africa; clayths@unisa.ac.za³ Inorganic Chemistry and Catalysis Division, CSIR-National Chemical Laboratory, Dr. Homi Bhabha Road, Pune 411008, India; tv.aswathy@ncl.res.in (A.T.V.); m.prabu@ncl.res.in (M.P.); t.raja@ncl.res.in (R.T.)⁴ Department of Chemistry, Nelson Mandela University, P.O. Box 77000, Port Elizabeth 6031, South Africa; adeniyi.ogunlaja@mandela.ac.za⁵ Academy of Scientific and Innovative Research (AcSIR), CSIR-HRDC Campus, Ghaziabad 201002, India

* Correspondence: ac_tella@yahoo.co.uk; Tel.: +234-803-501-9197

Abstract: The global demand on adipic usage in the production of plasticizers and synthetic polyamide is increasing. In line with the search for an efficient and energy-conserving way to isolate adipic acid (AA) in good yields, this paper introduces the oxidization of cyclohexanone utilizing two new coordination compounds, [Mn(2,6-pydc)₂](imi) (**1**) and [Co(H₂pza)₂(H₂O)₂(NO₃)]·NO₃ (**2**), as catalysts. Compounds **1** and **2** were synthesized by room temperature and refluxing methods, and characterized by spectral analyses (IR and UV-Vis.), SEM, BET, TGA, elemental, and X-ray crystallography. The single crystal structure of compound **1** revealed that pyridinedicarboxylate (2,6-pydc) and imidazole (imi) moieties were coordinated to the Mn(II) atom through imine nitrogen and deprotonated oxygen atoms, to form an undistorted octahedral coordination geometry with the N₂O₄ donor set. The axial and equatorial planes containing O₂, O₄, O₅, and O₇ atoms were from two adjacent 2,6-pydc ligands which formed the unidentate donor ligand; imi, on the other hand, acted as a bidentate donor ligand. For compound **2**, the Co(II) atom was being coordinated by two pyrazinamide (H₂pza) moieties, which acted as an unidentate donor ligand; two water molecules occupying the axial position, and one nitrate molecule occupying the apical position, were within the coordination sphere; a nitrate molecule was disordered outside the coordination sphere. The distance, 4.658 Å, between the Co1 atom and the N8 atom of the uncoordinated nitrate molecule, was within the range reported elsewhere. Cyclohexanone peroxidation experiments revealed that compound **1** exhibited unique catalytic performance by giving a 72.8% yield in adipic acid, in comparison to the 71.3% yield obtained with compound **2**. The yields in AA were maintained by way of recyclability evaluation. The reaction kinetics of compound **2** gave less activation energy, E_a 2938 J mol⁻¹, while the thermodynamic parameters indicated that the chemical reactivity of cyclohexanone on the active surfaces of compounds **1** and **2** was via monolayer physisorption.

Keywords: cyclohexanone; oxidation; pyrazinamide; pyridinedicarboxylate; imidazole; cobalt; manganese; complexes



Citation: Tella, A.C.; Isaac, A.Y.; Clayton, H.S.; Ogunlaja, A.S.; Venugopalan, A.T.; Prabu, M.; Thirumalaiswamy, R. Synthesis and Crystal Structures of Mn(II) and Co(II) Complexes as Catalysts for Oxidation of Cyclohexanone. *Inorganics* **2022**, *10*, 100. <https://doi.org/10.3390/inorganics10070100>

Academic Editors: Lars Öhrström, Susan Bourne and Francoise M. Amombo Noa

Received: 12 May 2022

Accepted: 3 July 2022

Published: 10 July 2022

Publisher's Note: MDPI stays neutral with regard to jurisdictional claims in published maps and institutional affiliations.



Copyright: © 2022 by the authors. Licensee MDPI, Basel, Switzerland. This article is an open access article distributed under the terms and conditions of the Creative Commons Attribution (CC BY) license (<https://creativecommons.org/licenses/by/4.0/>).

1. Introduction

The oxidation of KA oil (a mixture of cyclohexanol and cyclohexanone) in the presence of small amounts of metal complexes is reported to yield adipic acid (AA) [1,2]. The oxidation reaction usually takes place in chemical industries at high temperatures, and requires a two-step oxidation of cyclohexane or a one-step oxidation of cyclohexanol. The chemical industries also make use of nitric acid, which contributes to global warming, acid rain, and depletion of the ozone layer [3–5]. Moreover, advanced oxidation processes, which include oxidizing cyclohexane under UV light [6], oxidizing cyclohexane under an

oxygen gas medium [7], and carbonizing catalytic materials derived from lignocellulosic biomass also known as lignin-derived bio-oils [8], provide efficient and energy-conserving ways to prepare AA. According to reports, the bulk of these oxidation reactions are notably unsatisfactory, as low yields in AA are being achieved. The alternative use of aqueous hydrogen peroxide (H_2O_2) was related to a sustainable process, and has been widely adopted. Hydrogen peroxide slowly decomposes in a catalytic system, to form water as a byproduct at low temperatures [9,10].

Alcañiz-Monge, et al. [11], in 2014 reported the use of homogeneous (HPW, HPMo) and different heterogenous catalysts (PCoMo, PNiMo, PFeMo VPMo, $(\text{N}(\text{C}_3\text{H}_7)_4)_3\text{PMo}_{12}\text{O}_{40}$, $(\text{NH}_4)_3\text{PMo}_{12}\text{O}_{40}$, $\text{Cs}_3\text{PW}_{12}\text{O}_{40}$, and $(\text{NH}_4)_3\text{PMoO}_4$) for AA preparation with cyclohexene and 30% hydrogen peroxide; the reaction was performed in a batch reactor bed at 75 °C under autogenous pressure. The most active catalyst was found to be $\text{Cs}_3\text{PW}_{12}\text{O}_{40}$, as it gave an 80% yield of AA with acetic acid, while a 13% yield of AA was obtained in the absence of acetic acid. Moreover, Jianhui, et al. [12], developed a catalytic system with β -Anderson manganohexamolybdate containing a single-atom Mn active site; to enhance the AA preparation in a 30% H_2O_2 medium, cyclohexanone was adopted as the starting material. Considerable high conversion, selectivity, and turnover numbers (TON) (99%, 97%, and 2427.5 hr^{-1}) of AA were obtained.

The utilization of coordination compounds, such as metal complexes, and coordination polymers (metal–organic frameworks) for highly effective catalytic reactions, has been reported [13–21]. Coordination compounds are various types of compounds with metal ions—such as alkali and alkaline earth metals, transitional metals, and lanthanide(III) ions—coordinated by various functional groups, such as carboxylate, hydroxyl, and amine groups [21]. Several coordination compounds have shown intriguing catalytic activities owing to their flexibility, accessibility to surface acidity, possession of strong bonds between di- and trivalent metal ions and ligands pillared by nitrogen and oxygen atoms, superior stability, and resistance to decomposition upon heating. Reports, however, have revealed that the oxidation of cyclohexanone yields AA in pure form using coordination compounds [1,9,16].

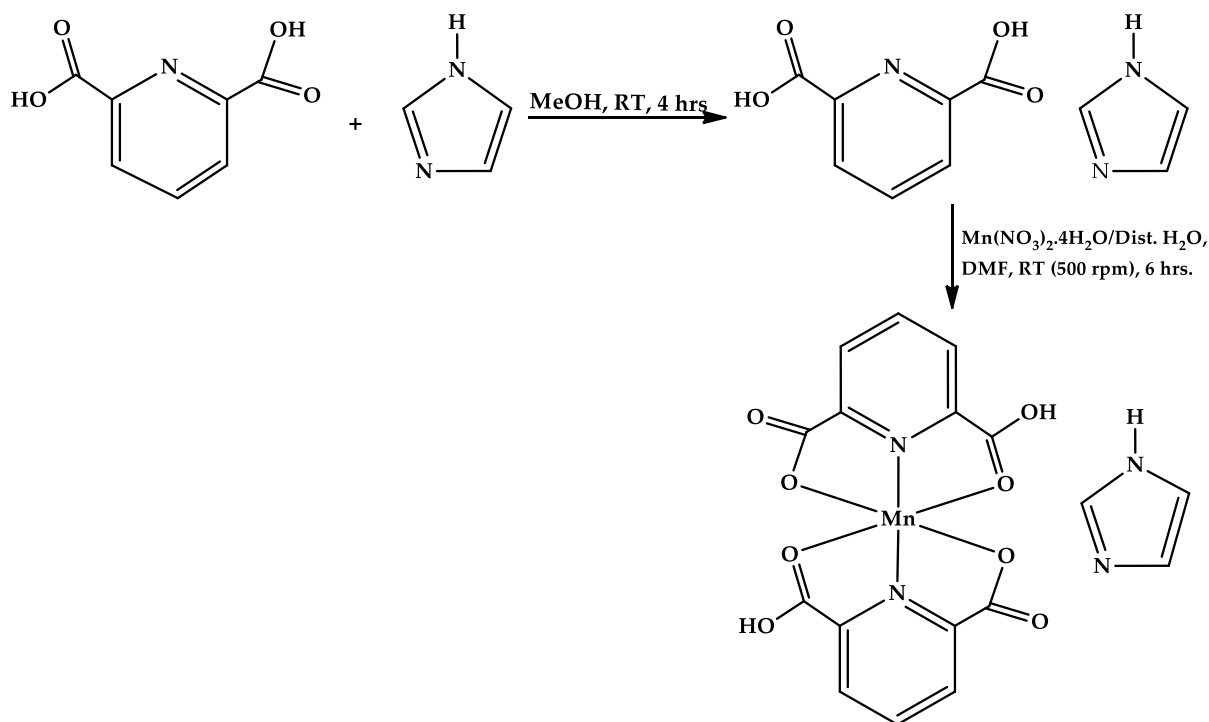
Furthermore, the global demand on adipic usage in chemical industries for the production of nylon-6,6, plasticizers, etc., is increasing [1,10]. The need to obtain AA in high yield and pure form is therefore imperative. Based on this premise, two new metal complexes, $[\text{Mn}(2,6\text{-pydc})_2](\text{imi})$ (1) and $[\text{Co}(\text{H}_2\text{pza})_2(\text{H}_2\text{O})_2(\text{NO}_3)]\bullet\text{NO}_3$ (2), were prepared as catalysts for the oxidation of cyclohexanone to AA in high yield and pure form. Both of the compounds utilized were chosen from Mn(II) ion, Co(II) ion, pyridylcarboxylate, azolate, and pyrazinamide ligands. The choice of ligands employed influenced the length, porosity, rigidity, and coordination modes on the resulting frameworks of coordination polymer material. These ligands consisted of adjustable linkers suitable for generating lower-dimensional coordination polymers. The synthesized materials were categorized into heterogeneous compounds, and as they exhibited good thermal behaviors, we selected them as being suitable for oxidizing a substrate like adipic acid [21]. Solvents were chosen from aqueous H_2O_2 and acetonitrile, because the yields of the products were between 60% and 90% in other literatures [20,21]. The effects of reaction temperature, time, and oxidants on the catalytic reactions, and the mechanism, kinetics, and thermodynamics of the reaction were studied in this research work.

2. Materials and Methods

All the reagents and solvents used in this study were of analytical grade, and required no further purification. Mn(II) ion salt, Co(II) ion salt, pyridylcarboxylate, imidazole, and pyrazinamide ligands were purchased from Sigma–Aldrich (USA) and Tokyo Chemical Industry (China). All the chemicals were used as received. FTIR and UV-visible spectra analyses were recorded on a SHIMADZU (Tokyo) FTIR-8501 spectrophotometer and a SHIMADZU UV-1650pc UV-VIS spectrophotometer. XRD analyses were performed on a PANalytical X'pert Pro dual goniometer diffractometer at 294 K, using $\text{CuK}\alpha$ radi-

tion ($\lambda = 1.54059$). Thermogravimetric analysis (TGA) of the complexes was performed on a Seiko (USA) DTA/TGA 320 instrument under air atmosphere at a heating rate of $10\text{ }^\circ\text{C min}^{-1}$ from 30 to 600 $^\circ\text{C}$. The % metal content of both catalysts was determined by EDAX (energy-dispersive absorption X-ray spectroscopy) analysis on an EDAX AMETEK (USA) Z2 Analyzer. HPLC analyses of the oxidation products and side products were carried out using a 1260 Infinity HPLC instrument made by Agilent Technologies (Santa Clara, CA, USA).

Synthesis of the co-crystals of (2,6-pydc–imi⁺): The synthetic procedure described by Gross, et al. [5], was modified and adopted for the synthesis of the co-crystals of (2,6-pydc–imi⁺). In a typical reaction, 2,6-pyridinedicarboxylic acid (2,6-pydc) (167.12 mg, 1 mmol) and imidazole (imi) (68.078 mg, 1 mmol) were dissolved separately in 25 mL beakers with 5 mL methanolic solution; thereafter, the two solutions were gently mixed together in a 25 mL beaker for about 1 min. The final solution was transferred to a 100 mL round-bottom flask, and stirred (at 500 rpm) for 4 h at room temperature (RT). The clear filtrate obtained was allowed to settle in a clean 20 mL vial, and then kept in the dark to allow formation of crystals. After 7 days, plate-like colorless co-crystals, suitable for single-crystal X-ray diffraction analysis, were formed (Scheme 1). The co-crystals were filtered off, washed with methanol, and dried in air for approximately 10 min.

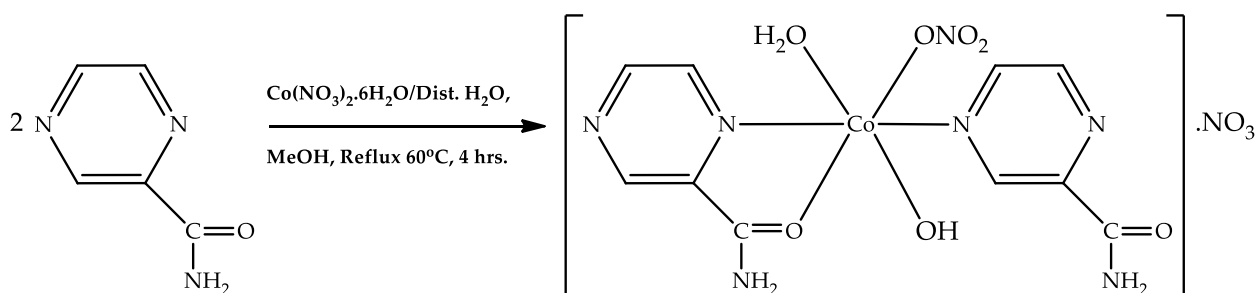


Scheme 1. Equation of reaction and structure of (2,6-pydc–imi⁺) and [Mn(2,6-pydc)₂](imi).

Synthesis of [Mn(2,6-pydc)₂](imi): The synthetic procedure described by Gross, et al. [5], was modified and adopted for the synthesis of [Mn(2,6-pydc)₂](imi). In practice, co-crystals of (2,6-pydc–imi⁺) (250 mg) were mechanochemically crushed to powder form, and later poured into a 20 mL vial where 5 mL DMF solution was added; the resulting solution was kept for 3 days in the dark; thereafter, manganese dinitrate tetrahydrate, Mn(NO₃)₂·4H₂O (251.01 mg, 1 mmol), already pre-dissolved with distilled water (5 mL) was added, and manually stirred for about 10 min. The mixture was transferred to a 100 mL round-bottom flask, and continuously stirred (500 rpm) for 6 h at room temperature (RT); the obtained grey filtrate was kept in the dark without any disturbance, for crystal growth to occur. Flake-like grey crystals suitable for single-crystal X-ray diffraction analysis were formed after 16 days. (Scheme 1). The mother liquor was decanted, and the crystals were filtered off, washed with ethanol, and dried in air for about 10 min. Yield: 60.2%, Mp. = 501 $^\circ\text{C}$,

Anal. Calc. for $C_{17}H_{10}MnN_4O_8$ (%): C, 43.43; H, 2.08; N, 7.24. Found %: C, 43.12; H, 2.41; N, 7.32. IR (KBr, ν/cm^{-1}): 1319, 1692, 1394, 1456, 1312, 663, 578. UV-Vis. (solid state diffuse-reflectance) (λ_{LMCT} , nm): 317; (λ_{d-d} , nm): 687.

Synthesis of $[Co(H_2pza)_2(H_2O)_2(NO_3)] \cdot NO_3$: The synthetic procedure described by Raja, et al. [14], was modified and adopted for the synthesis of $[Co(H_2pza)_2(H_2O)_2(NO_3)] \cdot NO_3$. In a typical reaction, pyrazinamide (H_2pza) (246.23 mg, 2 mmol) and cobalt dinitrate hexahydrate, $Co(NO_3)_2 \cdot 6H_2O$ (290.70 mg, 1 mmol), were dissolved separately in a 25 mL beaker with 5 mL methanolic solution and 5 mL distilled water. The two solutions were gently mixed together for about 30 s, and the mixture was refluxed in a 100 mL round-bottom flask at 60 °C for 4 h. Filtrate obtained from the refluxing mixture was allowed to stand freely on the bench without any disturbance for crystal growth formation. Block-like pink crystals, suitable for single-crystal X-ray diffraction analysis, were formed after 4 days (Scheme 2). The mother liquor was decanted, and the pink crystals were filtered off, washed with methanol, and dried in air (10 min). Yield: 52.5%, Mp. = 479 °C, Anal. Calc. for $C_{10}H_{14}CoN_8O_{10}$ (%): C, 28.66; H, 3.50; N, 24.34. Found %: C, 31.02; H, 3.58; N, 22.65. IR (KBr, ν/cm^{-1}): 1190, 1684, 782, 675. UV-Vis. (solid state diffuse reflectance) ($\lambda_{LLCT/LMCT}$, nm): 236, 272, 333; (λ_{d-d} , nm): 525.



Scheme 2. Equation of reaction and structure of $[Co(H_2pza)_2(H_2O)_2(NO_3)] \cdot NO_3$ (2).

3. Results and Discussion

The flake-like grey crystals of $[Mn(2,6-pydc)_2](imi)$ (1) were synthesized from the co-crystals of $(2,6-pydc-imi^+)$ via mechanochemical crushing, followed by adopting the room temperature synthetic method to obtain the product (Scheme 1); the yield was 60.2%. The block-like pink crystals of $[Co(H_2pza)_2(H_2O)_2(NO_3)] \cdot NO_3$ (2) were synthesized in good yield (52.2%) by refluxing pyrazinamide (H_2pza) and cobalt dinitrate hexahydrate with suitable solvent (Scheme 2); the stability temperatures, 287 °C and 140 °C, and melting point values, 501 °C and >470 °C, indicated their stability at high temperatures (see ESI for TGA estimation). The % metal content values (75.58% and 24.78%) was evaluated using MP-AES (microwave plasma-absorption emission spectroscopy), and predicted the presence of active metals (Mn and Co), respectively.

The physicochemical properties of 1 and 2 are summarized in Table 1.

Table 1. Physicochemical properties of $[Mn(2,6-pydc)_2](imi)$ (1) and $[Co(H_2pza)_2(H_2O)_2(NO_3)] \cdot NO_3$ (2).

Compound	Mp (°C)	Ts (°C)	%Metal Content EDAX (MP-AES)	C H% N%		
				Calculated (Found)		
1	501	287	-	43.43	2.08	7.24
				(43.12)	(1.61)	(6.32)
2	470	140	-	29.79	3.50	24.34
				(31.02)	(3.58)	(22.65)

Ts = stability temperature; Mp = melting point; EDAX = energy-dispersive X-ray spectroscopy; MP-AES = microwave plasma-atomic emission spectroscopy.

The FTIR spectrum result for 2,6-pydc showed a peak at 1181 cm^{-1} characteristic of the $\nu(C-N)$ band, and had shifted to 1319 cm^{-1} in the spectrum of compound 1 (see

Figure S1). This suggested the coordination of imine nitrogen to Mn(II) ion. The low-intensity peaks at 1709 cm^{-1} , 1256 cm^{-1} , and 3212 cm^{-1} were characteristic of $\nu(\text{C}=\text{O})$, $\nu(\text{C}-\text{O})$, and $\nu(\text{OH})$ bands in 2,6-pydc, and had shifted to 1692 cm^{-1} and 1394 cm^{-1} in the spectrum of compound **1**, confirming the coordination of the carboxylate oxygen atoms to the Mn(II) ion [21]. The hydrogen bond interactions between neighboring bonded atoms, i.e., imi and 2,6-pydc bearing N-H and OH groups, were confirmed by the disappearance of an $\nu(\text{OH})$ stretching band and the appearance of an $\nu(\text{C}-\text{N})$ weak band at 1295 cm^{-1} , respectively; these bands differed from those in the spectrum of **1** [22,23]. The separation ($\Delta\nu_{\text{COO}}$, 164) between $\nu_{\text{s}}\text{COO}$ and $\nu_{\text{as}}\text{COO}$ suggested that the carboxylate groups of 2,6-pydc exhibited bidentate bonding mode [21]. The characteristic peaks for the coordinated metal ions ($\nu_{\text{Mn}-\text{O}}$ and $\nu_{\text{Mn}-\text{N}}$ bands) appeared at 663 cm^{-1} and 578 cm^{-1} (Table S1).

For complex **2**, the FTIR spectrum of H_2pza displayed peaks at 1253 cm^{-1} and 1708 cm^{-1} characteristic of $\nu(\text{C}-\text{N})$ and $\nu(\text{C}=\text{O})$ stretching bands, and had shifted to 1190 cm^{-1} in the spectrum of **2** (see Figure S2); this indicated the involvement of Co(II) ion in coordination with pyrimidine nitrogen and carbonyl oxygen of H_2pza [24]. Furthermore, the two broad peaks, 3285 cm^{-1} and 3301 cm^{-1} —characteristic of trace amounts of water, $\nu(\text{OH}_{\text{w}})$, and amine $\nu(\text{NH}_2)_{\text{sy/asy}}$ stretching bands in the spectrum of the free ligand—had completely disappeared in the spectrum of **2**, suggesting the presence of hydrogen bonds between the NH_2 group, the coordinated H_2O , and the uncoordinated nitrate in **2** [24–26]. The peaks for the coordinated Co^{2+} ion, 782 cm^{-1} and 675 cm^{-1} , were characteristic of $\nu(\text{Co}-\text{O})$ and $\nu(\text{Co}-\text{N})$ bonds (Table S2).

The electronic spectrum for imi and 2,6-pydc showed three absorption bands, 230 nm, 277 nm and 280 nm, which were characteristic of imine nitrogen ($\text{C}=\text{N}$), carbonyl oxygen ($\text{C}=\text{O}$), and hydroxyl (OH) groups' chromophores within the cyclopentadiene and benzene rings of the parent ligands. These bands were assigned to $\pi \rightarrow \pi^*$ and $n \rightarrow \pi^*$ transitions. A shift to higher wavelengths, 317 nm and 687 nm, was observed near the visible region in the spectrum of compound **1** (Figure S3), probably due to ligand-to-metal charge transfer (LMCT) [22,23]. The band at 687 nm was attributed to a weak spin-forbidden transition, ${}^4\text{T}_{1\text{g}} \leftarrow {}^6\text{A}_{1\text{g}}$ (see Table S3), due to complexation between the Mn^{2+} ion and the O $\hat{\text{N}}$ donor atoms of 2,6-pydc [21].

For complex **2**, the electronic spectrum of the ligand (H_2pza) which exhibited absorption bands between 221–316 nm had shifted to 236–333 nm in the spectrum of **2** (Figure S4). These bands were characteristic of the imine ($\text{C}=\text{N}$), amine (NH_2), and carbonyl ($\text{C}=\text{O}$) groups' chromophores attached to the H_2pza benzene ring, and had been assigned to $\pi \rightarrow \pi^*$ and $n \rightarrow \pi^*$ transitions. The significant shifts in the spectrum of **2** near the visible region were due to ligand-to-metal charge transfer (LMCT). We tentatively assigned two low-intensity bands at 236 nm and 272 nm in the spectrum of **2** to a mixed LLCT/LMCT, due to less contributions of O $\hat{\text{N}}$ donor groups in H_2pza in the excited state [25]. In addition, the hyperchromic shift, 525 nm, observed at the visible region in the spectrum of the complex, was assigned to ${}^4\text{A}_{2\text{g}} \rightarrow {}^4\text{T}_{1\text{g}}$ (P) transition (see Table S4), due to d-d* transition of the d^7 system of Co(II) cation. The effect of the hyperchromic shift was attributed to complexation between Co^{2+} and H_2pza .

Thermogravimetric analysis was conducted under nitrogen atmosphere, at a maximum temperature of $600\text{ }^\circ\text{C}$. The TG curve of **1** (Figure S5) indicated a starting stepwise weight loss in the range of $228\text{--}357\text{ }^\circ\text{C}$, which corresponded to the decomposition of uncoordinated imi moiety (mass loss was 43.1%/44.8% for calc./found). A second-stage weight loss was in the range of $366\text{--}505\text{ }^\circ\text{C}$, which corresponded to the decomposition of 2,6-pydc bound to Mn(II) ion in the chemical structure (mass loss was 17.5%/20.3% for calc./found). The final stage of thermal decomposition was between $506\text{--}600\text{ }^\circ\text{C}$, which was attributed to MnO residue formation. The thermal decomposition behavior of **2** (Figure S6) also revealed a weight loss in the range of $125\text{ }^\circ\text{C}$ to $365\text{ }^\circ\text{C}$, which corresponded to: (i) the decomposition of uncoordinated (lattice) nitrate molecules; (ii) coordinated nitrate molecules; and (iii) coordinated water molecules. The mass loss of nitrate(s) was found to be 5.3/10.3% (calc./found), while that of water molecule(s) was given as 4.4/5.6%

(calc./found). The mass loss which occurred in the range of 366 °C and 471 °C was attributed to the decomposition of the H₂pza organic specie; experimental mass loss was found to be 34.0/30.5% (found/calc.). The final stage of thermal decomposition started from 472 °C down to 600 °C, and was ascribed to the formation of CoO residue (metal oxide). The thermal stability (>228 °C and >128 °C) observed in **1** and **2** suggested that both compounds would serve as good catalyst materials, and these results were comparable to those of 2,4-pyridinedicarboxylato triaqua cadmium(II) hemihydrate, Co²⁺, and Cd²⁺ containing pyrazinamide, reported elsewhere [21,26–28].

3.1. Description of the Crystal Structure of [Mn(2,6-pydc)₂](imi) (**1**) and [Co(H₂pza)₂(H₂O)₂(NO₃)]•NO₃ (**2**)

The crystal data collection and structure refinement parameters for the cocrystals and crystals of compounds **1** and **2** are highlighted in Table S5.

[Mn(2,6-pydc)₂](imi) **1** crystallized in the orthorhombic Pbc_a space group, with the asymmetric unit consisting of one Mn(II) atom bound by two 2,6-pydc molecules, and one molecule of imidazole lying outside the coordination sphere (see Figure 1). The central Mn(II) atom lay in an undistorted octahedral coordination environment with an N₂O₄ donor set; the adjacently-coordinated 2,6-pydc ligands, containing O2, O4, O5, and O7 atoms, were constructed in such a way that both occupied the axial and equatorial planes. Each of the 2,6-pydc carboxylate groups exhibited the μ₁-η¹:η⁰-monodendate coordination mode [22,27]. The [Mn(COO)₂] structural building unit (SBU) could be considered as a 2-connected node, in which the Mn(II) sat on an inversion center, and was defined by four carboxylate oxygen atoms, which formed a finite two-dimensional (2D) structure.

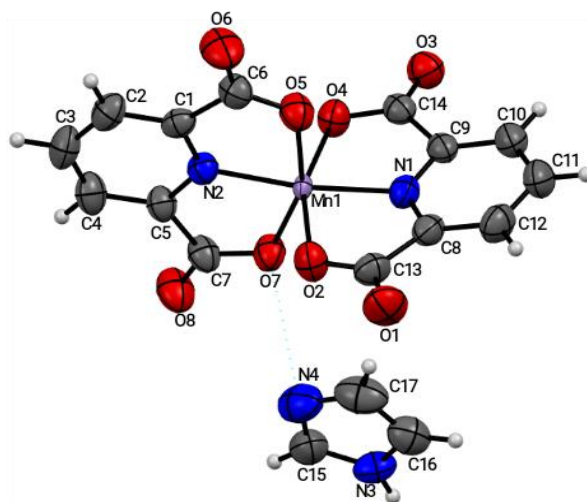


Figure 1. ORTEP diagram of **1** (010). Red = oxygen, Blue = nitrogen, Grey = carbon, Purple = manganese.

In addition, the uncoordinated imidazole molecule, situated at the equatorial plane outside the coordination sphere, was linked to the framework by hydrogen bond interactions via N4 and N3 (calc. distance = 3.012 Å). The hydrogen bond and/or van der Waals' interactions between the uncoordinated imidazole and the coordinated 2,6-pydc were labeled as N3–H3a···O3 and O7···N4; these bonds stabilized the two-dimensional (2D) structure of compound **1** (see Figure S7). It was also evident that O7···N4 constituted the van der Waals' contact. The hydrogen bond parameters for [Mn(2,6-pydc)₂](imi) are shown in Table S6. Furthermore, the position of the Mn1–O2 (2.000 Å) and Mn1–O4 (2.011 Å) bonds, of one 2,6-pydc[−] moiety, were in a normal range with those of the adjacent Mn1–O5 (2.023 Å) and Mn1–O7 (1.998 Å) bonds, indicating that the assigned Mn–O bond energies were perpetually the same (Figure S3). Similarly, the O2–Mn1–O4 (157.90°) angle of one 2,6-pydc[−] moiety occupying an axial position deviated by a small angle of ca. 0.21° from the O5–Mn1–O7 (157.69°) of the adjacent 2,6-pydc moiety, showing that the angles were in

plane, and that there was bite distortion from the linearity [27]. Distances of 1.957 Å and 1.971 Å between the (Mn1-N1) and (Mn1-N2) bond were shorter than the Mn1–O bonds (bond range was from 1.998 Å to 2.023 Å), indicating that the bond energies, E_b between the Mn^{2+} –N atoms (of 2,6-pydc), were stronger than the Mn^{2+} –O atoms of 2,6-pydc [29]. The selected bond distance and angles of compound 1 are presented in Table S7.

The crystal structure of $[Co(H_2pza)_2(H_2O)_2(NO_3)] \cdot NO_3$ (2) in Figure 2 crystallized in the triclinic P-1 space group, with one Co(II) metal atom, two pyrazinamide (H_2pza) molecules, two water molecules, and two nitrate molecules in the asymmetric unit. The crystal structure revealed also that the cobalt ion was being coordinated by: (i) two H_2pza molecules acting as the unidentate donor ligand; (ii) two water molecules; and (iii) one nitrate molecule within the coordination sphere, which provided the counter ion for the Co^{2+} atom; the uncoordinated nitrate molecule also provided the counter ion to enhance the rigidity (stability) of the framework. The resulting oxidation state of the cobalt ion in the crystal structure was +2 [25].

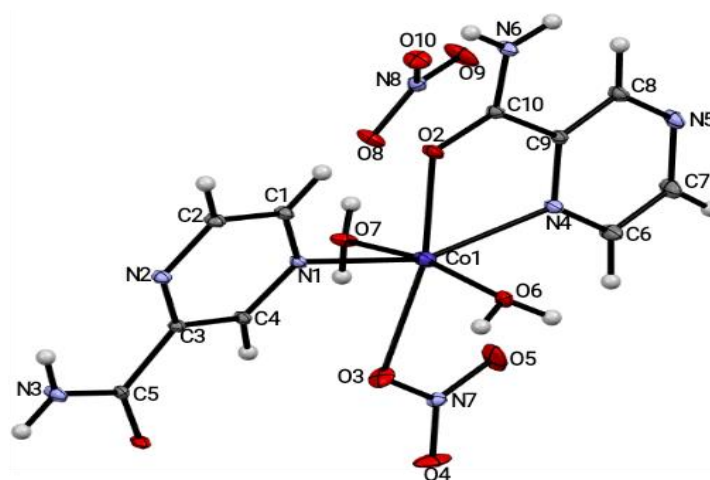


Figure 2. ORTEP diagram of 2 (010) showing atoms numbering. Red = oxygen, Purple = nitrogen, Grey = carbon, White = hydrogen, Blue = Cobalt.

The average bond length of Co1–N was 1.8070 Å, while that of Co1–O was 2.1968 Å, respectively. This observation was similar to the average bond lengths of Co–N and Co–O found for copper (II) bound by pyrazinamide and 2-nitrobenzoate [24]. The bond angles of O–Co1–N ranged from 80.26(5)° to 125.44(5)°, while O–Co1–O ranged from 84.25(5)° to 97.57(6)°, respectively. The average bond length of Co–O (2.1968 Å) suggested that the bond energies (E_b) between Co–O were weaker than those of Co–N [21,30]. Selected bond lengths and bond angles in compound 2 are highlighted in Table S8.

The distance, 4.658 Å, between the Co1 atom and the N8 atom of the uncoordinated nitrate molecule was within the range reported for other coordination polymers [25]. The coordinated water molecules were bound to the Co^{2+} ion by ionic bonds, and formed pendants for the 1D structure along the crystallographic *b* plane, as shown in Figure 3.

The 1D structure showing hydrogen bonds in Figure S8 indicates that the free nitrate and coordinated water molecules formed a network of hydrogen bonds, in which the linkers (hydrogen bonds) ran along the *c*-axis in the direction of the coordinated nitrate, and along the *a*-axis in the direction of the free nitrate and coordinated water molecules [25]. Furthermore, the intra-molecular hydrogen bond interactions in compound 2 involved those of aromatic amine, carbonyl groups, coordinated nitrate, O6W, and O7W, and they were labeled as (O6–H6C···O1), (O6–H6D···O3), (O7–H7A···O1), and (N3–H3B···N5), respectively. The inter-molecular hydrogen bond interactions involved those of aromatic amine groups, O7W, and free nitrate, and they were labeled as (O7–H7B···O8), (N3–H3A···O10), and (N6–H6B···O9). The parameters for the intra- and inter-molecular hydrogen bond interactions are summarized in Table S9.

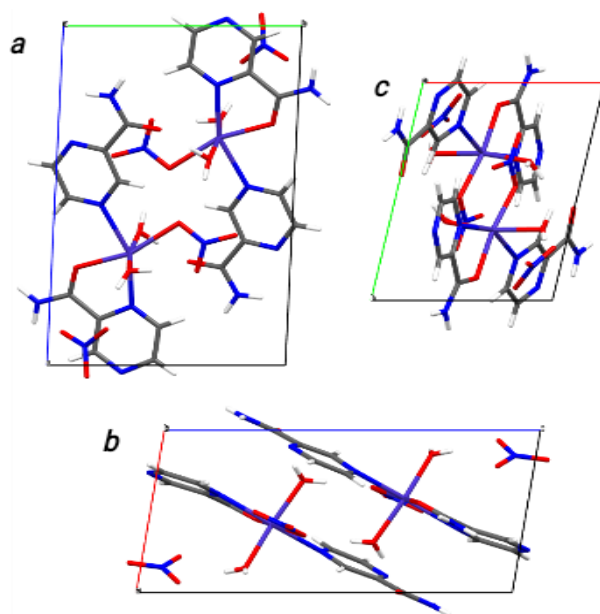


Figure 3. 1D structure showing packing arrangements of compound **2** along the crystallographic (a)–(c) planes.

3.2. Powder X-ray Diffraction Patterns (PXRD) of $[Mn(2,6\text{-pydc})_2](\text{imi})$ (**1**) and $[\text{Co}(\text{H}_2\text{pza})_2(\text{H}_2\text{O})_2(\text{NO}_3)] \bullet \text{NO}_3$ (**2**)

Powder XRD patterns (Cu, $K\alpha$) of compounds **1** and **2** (Figures S9 and S10) were conducted, to probe the characteristic phases related to the active sites in both materials prior to their usage as catalysts. Both samples were activated at 100 °C prior to catalytic application. However, the simulated PXRD patterns of compounds **1** and **2** displayed characteristic diffraction phases, with very slight variation where peaks disappeared for the as-synthesized patterns. The simulated patterns of compounds **1** and **2** displayed peaks at $2\theta = [11.4^\circ, 12.2^\circ, 12.9^\circ, 14.2^\circ, 22.9^\circ, 23.7^\circ, 26.4^\circ \text{ and } 30.4^\circ]$, and $2\theta = [6.3^\circ, 11.9^\circ, 13.3^\circ, 15.5^\circ, 16.4^\circ, \text{ and } 23.6^\circ]$, which corresponded to [(100), (004), (102), (112), (200), (211), (222), and (233)] and [(001), (011), (100), (101), (012), and (112)] planes; these were typical of MnO and CoO accessible sites, respectively. Furthermore, it was observed that the PXRD patterns of compounds **1** and **2** in crystalline powder form were consistent with the simulated pattern in single-crystal form; this implied that the structural integrity of both materials was retained after crushing to powder form [31].

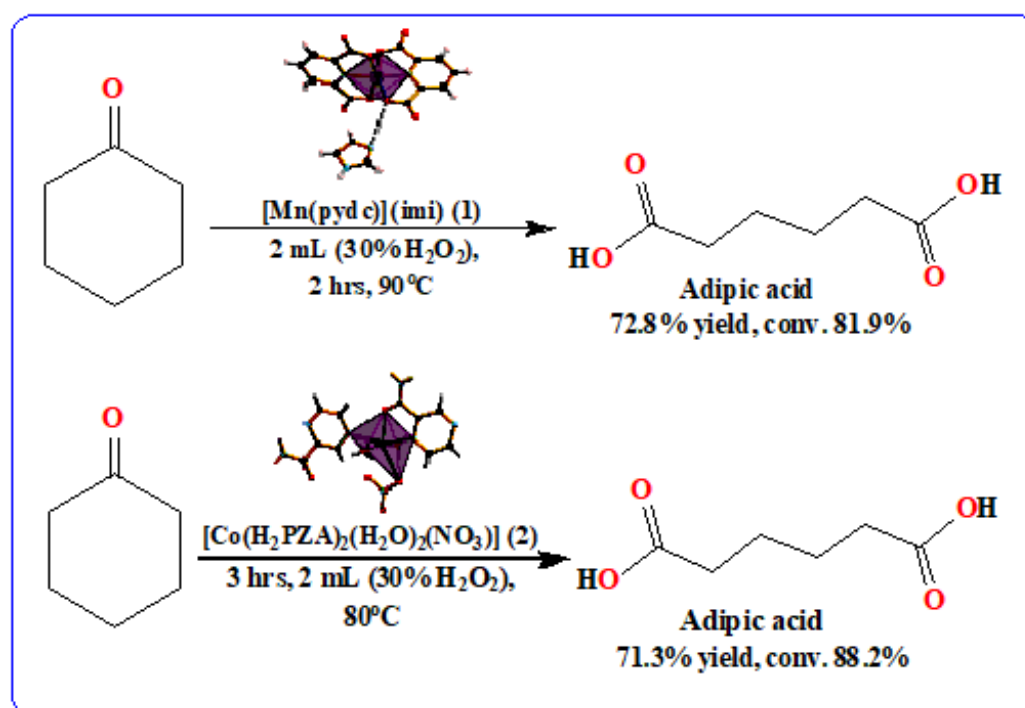
3.3. High Resolution (HR) TEM Images of **1** and **2**

The TEM images of compound **1** scanned at 100 nm and 0.2 μm revealed flake-shaped morphology consisting of pore walls attributed to crystallites co-assembling to form a moderate ordered mesostructure. The TEM images of compound **2** were scanned at 20 nm and 100 nm, and gave block-shaped morphology; the inset (selected area electron diffraction, SAED) illustrates that crystallinity (spots) and Bragg's reflection were from an individual crystallite [22]. The HRTEM images of compounds **1** and **2** are shown in Figure S11A,B, respectively.

4. Oxidation of Cyclohexanone

The strong pre-adsorption of cyclohexanone on a catalyst's surface is an important phenomenon for an efficient chemical transformation to take place, as it affects the rate and mechanism of transformation [2,9]. For this reason, before examining the catalytic activity of each compound, thermal stability tests were performed, using the TG analytical technique. In addition, thermal activation of the samples was carried out at 100 °C under vacuum in air. Thermal activation of each sample was done to: (i) remove lattice water and

other uncoordinated molecules; and (ii) generate the coordinatively unsaturated metal sites (acidic sites). The typical reaction scheme for the catalytic process is illustrated in Scheme 3.



Scheme 3. Oxidation of cyclohexanone catalyzed by Mn(II) catalyst.

Compounds 1 and 2, with different ligands, were able to catalyze each reaction, such that the +2 oxidation states of the metals were retained. The use of one or two ligands provided high selectivity to AA. The isolated yields of AA, as shown in Scheme 3, indicated that the use of the Mn-coordinated compound (1) gave a 72.8% yield of AA, while compound 2, acting as Co^{2+} catalyst, gave a 71.3% yield of AA. The side products obtained gave very low yields, such as 6-hydroxyhexanoic acid and ϵ -caprolactone. Furthermore, it was observed that the thermal activation of each candidate material enhanced their hydrolytic stability, and favored the catalytic activity of both compounds. The oxidation of cyclohexanone was also promoted with the use of 30% H_2O_2 . The selected catalytic activity of both complexes under study is summarized in Table 2 below.

Control experiments were performed at 30°C and at temperatures above 100°C , giving low yields, (21.0% and 36.6%), of AA. This suggests less activation energy input at 30°C and poor performance catalysts at temperatures above 100°C due to defects in active sites. By observation, an appreciable yield of AA was obtained over the Mn(II) and Co(II) catalysts (1), on the basis that there was a complete charge balancing by the acidic ligands, and formation of a water soluble complex which made contact with an oil phase (cyclohexanone) [2]. It was suspected also that the conversion of cyclohexanone to AA was favored by acetonitrile, which prevented water from accessing the active sites of both catalysts; this enhanced mass transfer, and resulted in an accelerated reaction rate [32]. The catalysts also appeared to be retained within the solution through multiple cycles of re-use, and were not dissolved in water; in other words, the structural integrity of both complexes was retained. The effects of other factors on the reaction were studied as follows.

Table 2. Selected catalytic activity of compounds **1** and **2** for cyclohexanone oxidation.

Entry	Cat.	Cat. Amount (mol L ⁻¹)	Conversion ^a (%)	Yield (%)	TON	TOF (h ⁻¹)	AA	Selectivity Capro	6-Hx	Others
1 ^b	1	0	0.3	1.2	0.2	0.0	trace	trace	trace	>99.0
2	"	7.4 × 10 ⁻⁴	18.2	12.3	12.7	6.4	20.2	-	-	69.8
3	"	1.4 × 10 ⁻³	42.1	64.0	29.5	14.8	38.4	8.0	2.0	-
4	"	2.2 × 10 ⁻³	54.9	46.0	38.4	19.2	69.3	23.0	-	7.7
5	"	2.9 × 10 ⁻³	81.9	72.8	57.4	28.7	64.1	3.6	7.6	>14.0
6 ^{bc}	2	0	0.7	1.2	0.1	0.0	trace	trace	trace	>99.0
7	"	7.1 × 10 ⁻⁴	17.6	25.2	4.2	1.4	45.0	15.4	12.1	>60.0
8	"	1.4 × 10 ⁻³	48.7	36.0	11.6	3.8	31.9	18.9	-	-
9	"	2.1 × 10 ⁻³	88.2	71.3	55.6	18.5	67.2	8.5	13.4	-
10	MnN	4.0 × 10 ⁻³	9.3	12.5	6.3	2.1	23.6	-	-	-
11	CoN	7.1 × 10 ⁻⁴	7.9	22.1	4.9	1.6	14.5	-	-	-
12 ^c	1	2.9 × 10 ⁻³	17.3	17.8	12.1	6.1	34.5	-	-	-
13 ^d	"	2.9 × 10 ⁻³	53.7	13.6	37.6	18.8	10.9	-	-	-
14 ^c	2	2.1 × 10 ⁻³	29.9	22.7	20.9	6.9	32.5	-	-	-
15 ^d	"	2.1 × 10 ⁻³	65.2	48.1	45.7	15.2	15.2	-	-	-

Reaction conditions: Catalyst **1** amount (7.4 × 10⁻⁴ mol L⁻¹), 80 °C, 2 hrs; Catalyst **2** amount (7.1 × 10⁻⁴ mol L⁻¹), 80 °C, 3 hrs; 1 mL of 0.0394 wt% cyclohexanone in CH₃CN/water, 4 mL of H₂O₂ (30% aqueous, 170.4 mmol), AA: Adipic acid, Capro: ε-Caprolactone, 6-Hx: 6-Hydroxyhexanoic acid, ^a Cyclohexanone conversion based on cyclohexanone consumed, ^b Yields measured in the absence of catalyst (b and b), ^c Yields measured after 40 min. of reaction, ^d Yields measured with 2 mL solution of H₂O₂, (30% aqueous, 85.2 mmol). Others: cyclohexanone peroxide and water; MnN = Mn(NO₃)₂·4H₂O; CoN = Co(NO₃)₂·4H₂O; Cat. = catalyst; TON = No. of moles of reactant converted ÷ moles of metal ion; TOF = No. of moles of reactant converted ÷ moles of catalysts and time (h).

4.1. Effect of Reaction Temperature

The experiment was initially performed at low temperature, 40 °C, giving low conversions of cyclohexanone [Table 2, Entries 2 and 7]. This was attributed to the limited catalytic activity of compounds **1** and **2** at low temperatures. The isolated yields of AA increased as the reaction temperature was increased gradually, by observation. Optimum yields of AA (72.8% and 71.3%) were recorded at 80 °C [Table 2, Entries 5 and 9]; this suggests the practical applicability of Mn(II)- and Co(II)-coordinated compounds to accelerate the direct conversions of cyclohexanone (81.9% and 88.2%). The selectivity of AA was 64.1% and 67.2%, respectively, in the presence of H₂O₂ at 80 °C. Furthermore, the use of deionized (DI) water, i.e., 41.6% at 40 °C, increased the liquid yield of caprolactone peroxide, while the measurement of 20.8% of DI favored the target product yields [Table 2, Entries 2 and 7] [4,33]. The TOF of the oxidation reactions at different reaction temperatures was 40 °C (6.4 h⁻¹ @**1** and 1.4 h⁻¹ @**2**) < 50 °C (14.7 h⁻¹ @**1** and 4.9 h⁻¹ @**2**) < 60 °C (16.3 h⁻¹ @**1** and 5.4 h⁻¹ @**2**) < 70 °C (22.7 h⁻¹ @**1** and 7.3 h⁻¹ @**2**) < 80 °C (28.7 h⁻¹ @**1** and 18.5 h⁻¹ @**2**), respectively. The graphical illustration for the effect of the reaction temperature is shown in Figure S12.

4.2. Effect of Catalyst Loading

As varying degrees of temperature affect the performance of a catalyst, the amounts of catalysts loaded into the catalytic systems were studied. In one of the experiments, the absence of catalysts gave only a traceable amount of AA over compounds **1** and **2** [Table 2, Entries 1 and 6]; this indicated the dependence of the reaction on active species present in the catalytic system, i.e., Mn²⁺ and Co²⁺ ions [29]. An HPLC chromatogram of a product (traceable amount of AA, 2 μL), taken and analyzed in the absence of catalyst **1**, has been shown in Figure S13. The use of Mn(NO₃)₂·4H₂O (MnN) and Co(NO₃)₂·4H₂O (CoN) were also examined; these gave very low yields of AA (12.5% over compound **1**, and 22.1% over compound **2**) [Table 2, Entries 10 and 11]. However, the oxidation of cyclohexanone over low amounts of compounds **1** and **2** (1.4 × 10⁻⁴ mol L⁻¹) gave moderate yields: 64.0%

and 48.7% of AA [Table 2, Entries 3 and 8]. There were improved product yields, 72.8% and 88.2%, when the amounts of catalysts were slightly increased [Table 2, Entries 5 and 9]. This also suggests the dependence of the reaction on more Lewis acidity coverage with respect to the bulk solution, thereby enhancing the inter-cavity diffusion of cyclohexanone through the catalysts' pore walls [26,34,35]. The TOF of the oxidation reactions of different loading was $0.00074 \text{ mol L}^{-1}$ (6.4 h^{-1} @1) < $0.0014 \text{ mol L}^{-1}$ (14.8 h^{-1} @1) < $0.0022 \text{ mol L}^{-1}$ (19.2 h^{-1} @1) < $0.0029 \text{ mol L}^{-1}$ (28.7 h^{-1} @1) and $0.00071 \text{ mol L}^{-1}$ (1.4 h^{-1} @2) < $0.0014 \text{ mol L}^{-1}$ (3.8 h^{-1} @2) < $0.0021 \text{ mol L}^{-1}$ (18.5 h^{-1} @2), respectively. An illustration of the effect of catalyst loading on the oxidation of cyclohexanone is presented in Figure S14.

4.3. Effect of Reaction Time

An experiment was conducted at the reaction time of 40 min on compounds 1 and 2, which gave 17.8% and 22.7% yields of AA [Table 2, Entries 12 and 14]. As the reaction progressed by gradually increasing the time, the full catalytic potentials of compounds 1 and 2 were released, giving optimum conversions/selectivity of AA (81.9%/64.1% and 88.2%/67.2%) after 2 and 3 hrs, respectively, [Table 2, Entries 5 and 9]. The TOF of the oxidation reaction at variable times was 40 min. (6.1 h^{-1} @1 and 6.9 h^{-1} @2) < 120 min (28.7 h^{-1} @1) < 180 min (18.5 h^{-1} @2), respectively. The graphical illustrations for the conversion of cyclohexanone at different reaction times are shown in Figure S15A,B. The HPLC chromatogram of AA attributed to the maximum activity of compound 1 on the reaction system is shown in Figure S16. These results are consistent with those reported elsewhere [3,36].

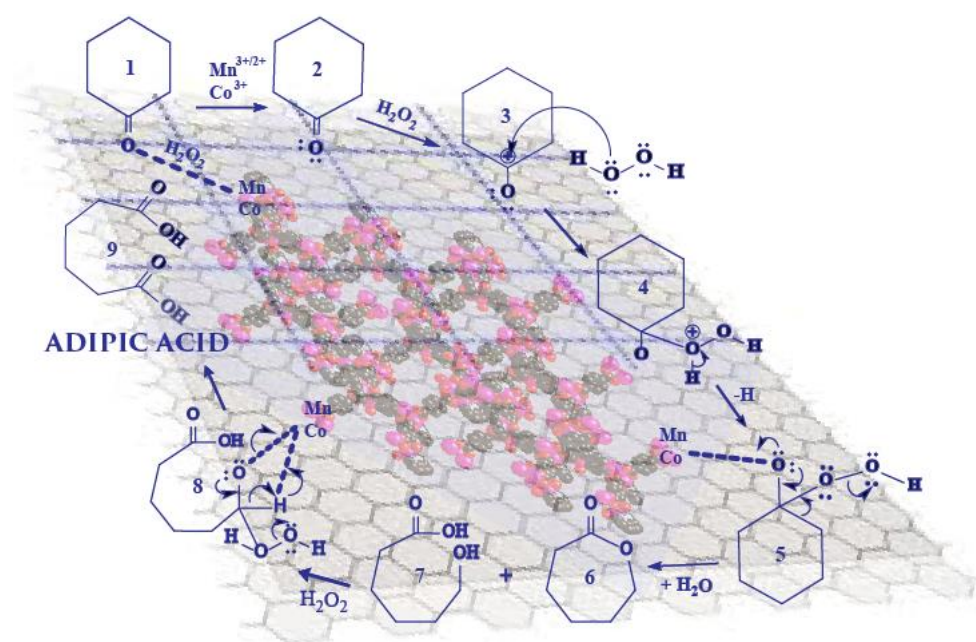
4.4. Effect of Oxidant

The effect of oxidant on the catalytic performance of compounds 1 and 2 was monitored by reacting mixtures in the absence of oxidant, H_2O_2 . The quantified amounts of AA were not promoted by this attempt. However, 53.7% and 65.2% conversions of cyclohexanone were recorded with 85.2 mmol of H_2O_2 [Table 2, Entries 13 and 15]. Optimum yields of AA, 72.8%, and 71.3%, were also recorded with the use of 170.4 mmol of H_2O_2 after 2 and 3 hrs of reaction time over compounds 1 and 2, respectively, [Table 2, Entries 5 and 9].

Tella, et al. [32], reported the formation of by-product of water molecules during the decomposition of H_2O_2 , which could be attributed to the conversions, 53.7% and 65.2%, recorded with H_2O_2 , 85.2 mmol.

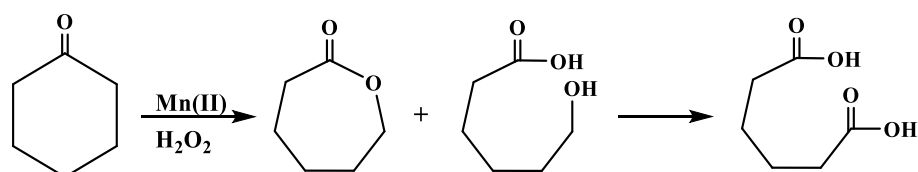
Furthermore, investigation of UV-visible spectral analysis of reactive systems containing compounds 1, 2, and oxidant (H_2O_2) were carried out in the presence and absence of cyclohexanone. Studies showed that the reactive species, Mn and Co, gave characteristic absorption bands in the absence of cyclohexanone, at a constant temperature of 80°C at 240 nm ($\pi \rightarrow \pi^*$), 370 nm ($n \rightarrow \pi^*$), and 512 nm (d-d transition) for compound 1; and 264 nm ($\pi \rightarrow \pi^*$), 361 nm ($n \rightarrow \pi^*$), and 722 nm (d-d transition) for compound 2 (Figure S17, 1a and 2a); this was attributed to Mn(II)- H_2O_2 and Co(II)- H_2O_2 adducts formation. Reduced concentrations of compounds 1 and 2 were traceable to the addition of cyclohexanone, leading to a slight decrease of spectral intensity at 512 nm for compound 1 (Figure S17; 1b), and the disappearance of spectral band, coupled with a slight shift of the spectral band from the initial 722 nm to 734 nm for compound 2 (Figure S17; 2b). This was attributed to the formation of Mn- H_2O_2 -cyclohexanone and Co- H_2O_2 -cyclohexanone intermediates or adducts, due to reactive species oxidization from Mn(II) and/or Co(II) to Mn(III/II) and/or Co(III) in H_2O_2 medium via the enhanced charge transfer mechanism, before completing the catalytic process [32,36].

Xia, et al. [37] also reported a mechanism called Baeyer–Villiger oxidation, which has been used to describe the oxidation of cyclohexanone with H_2O_2 in different systems. The modified reaction mechanism is comprised of steps 1 to 9, as shown in Scheme 4 below.



Scheme 4. Schematic representation of the mechanism for cyclohexanone oxidation over compounds 1 and 2. Steps 1–5 involve catalytic activation, charge transfer and adsorption of cyclohexanone onto the catalysts' surface via oxidation of H_2O_2 to form ϵ -caprolactone; steps 5–8 involve desorption reaction and decomposition of H_2O_2 ; and further desorption reaction to form 6-hydroxyhexanoic acid; step 9 involves formation of adipic acid.

Mn(II) and Co(II) was first activated via enhanced oxidation in an H_2O_2 medium, to form active $\text{Mn(III/II)-H}_2\text{O}_2$ and $\text{Co(III)-H}_2\text{O}_2$ adducts (steps 1 and 2) [32]. Charge transfer occurring from $\text{Mn-H}_2\text{O}_2$ and $\text{Co-H}_2\text{O}_2$ resulted in the diffusion of cyclohexanone onto an active surface (catalyst) to form reactive $\text{Mn-H}_2\text{O}_2$ -cyclohexanone and $\text{Co-H}_2\text{O}_2$ -cyclohexanone intermediates. The adsorbed cyclohexanone underwent rearrangement and/or breaking of bonds (steps 3 and 4), followed by decomposition of H_2O_2 in step 4, which formed OH^\bullet and CyOO^\bullet radicals. Deprotonation of a hydrogen ion and desorption reaction in step 5 led to the formation of ϵ -caprolactone, and water as a byproduct of the decomposition of the H_2O_2 . Further desorption reaction led to the formation of 6-hydroxyhexanoic acid in step 6, while continual activation of 6-hydroxyhexanoic acid in the H_2O_2 medium (steps 7 and 8) favored the formation of AA in step 9. The quantification of the reaction products was in good agreement with those reported elsewhere [2,19]. The TOF of the reaction with H_2O_2 was $85.1 \text{ mmol (18.8 h}^{-1} \text{ @1 and 15.2 h}^{-1} \text{ @2)} < 170.4 \text{ mmol (28.7 h}^{-1} \text{ @1 and 18.5 h}^{-1} \text{ @2)}$, respectively. The illustration for the formation of the two intermediates is as shown in Scheme 5.



Scheme 5. Illustration of the two intermediates formed as by-products in the oxidation of cyclohexanone.

The target product (2 μL) was authenticated by conducting ^1H NMR and ^{13}C NMR spectroscopic analyses. The ^1H NMR signal (Figure S18) at optimum reaction conditions revealed chemical shifts at 3.26–3.70 δ (ppm), and was assigned to methylene protons $\text{CO-(CH}_2)_n\text{-CO-}$ of AA; this was denoted as 'b' and 'c'. The signal for aliphatic protons attached to carboxylate groups (C=O-OH) appeared at 11.96 δ (ppm), and was denoted as 'a'.

Similarly, the ^{13}C NMR spectrum shown in Figure S19 revealed two sharp signals at 20.34 δ (ppm) and 34.27 δ (ppm), which were assigned to methylene carbon atoms, $(-\text{CH}_2)_n$. These were also denoted as 'b' and 'c'. The carbon atoms attached to the carboxylate group displayed signals at 179.82 δ (ppm), and were denoted as 'a'. Both the ^1H and ^{13}C NMR spectra reported herein were comparable to those reported in the literature [23].

Jianhui, et al. [12], compared the product selectivity (mol %) of KA oil in oxidation with H_2O_2 over metal catalysts, as a basis for recyclability evaluation; the result of our studies indicated that the isolated yield in adipic acid was maintained after the first and second cycle of reuse. A loss in catalytic activity was observed after the third cycle of reuse, due to a coordinative mismatch between the metal nodes and linkers, and the inherent Lewis acidity defects (Figure S20) [14].

MP-AES analysis was further carried out to ascertain the active metal contents in both compounds (Table 3). The results gave low Mn^{2+} and Co^{2+} contents in compounds 1 and 2, suggesting a reduced number of coordinatively unsaturated sites (CUM) [14,28].

Table 3. MP-AES analysis of Mn and Co contents in compounds 1 and 2 before and after recyclability tests.

Compound	Before ox.	% Mn and Co contents (MP-AES)		
		1st Use	2nd Reuse	3rd Use
72.58	69.01	66.27	62.12	56.34
24.78	22.19	20.15	17.03	11.11

MP-AES = microwave plasma-absorption emission spectroscopy; ox. = oxidation.

5. Kinetics and Thermodynamics of Cyclohexanone Oxidation

The kinetics of cyclohexanone-catalyzed reactions were studied by following a theoretical study by Kumal, et al., 2008 [38]. The rate law, using the Langmuir–Hinshelwood (L-H) mechanism, of the unimolecular reaction was expressed as:

$$\frac{1}{r} = \frac{1}{k_1[A]} + \frac{k_{-1}}{k_1k_2}$$

where r = rate of reaction, $[A]$ = final concentration of cyclohexanone, k_1 = adsorption rate constant, k_{-1} = desorption rate constant, and k_2 = decomposition rate constant. The slope and intercept corresponded to the above rate constants, and was obtained in an L-H linear plot of $1/r$ vs. $1/[A]$. The L-H plot obtained from this study is presented in Figure S21.

The L-H plot parameters obtained for the oxidation of cyclohexanone are summarized in Table 4 below:

Table 4. Langmuir–Hinshelwood (L-H) plot parameters for the oxidation of cyclohexanone over compounds 1 and 2.

Catalyst	k_1/s^{-1}	k_{-1}/s^{-1}	k_2/s^{-1}	K^\ddagger	K^*	$r/\text{M s}^{-1}$	R^2
1	1.51×10^{-4}	-3.04×10^{18}	5.84×10^{15}	-2.01×10^{22}	-1.17×10^{38}	1.67×10^{-7}	0.9968
2	9.49×10^{-5}	-3.62×10^{18}	5.84×10^{15}	-3.81×10^{22}	-2.23×10^{38}	1.00×10^{-7}	0.9945

@Compound 1, $T = 80^\circ\text{C} \pm 1^\circ\text{C}$; time, $t = 40$ to 120 min—converted to seconds; @Compound 2, $T = 80^\circ\text{C} \pm 1^\circ\text{C}$; time, $t = 40$ to 200 min—converted to seconds; r = rate of reaction; K^\ddagger = equilibrium constant; K^* = overall rate constant.

In Table 4, it is evident that the regression coefficient values, R^2 , suit the L-H model used for describing the adsorption process [38,39]. The positive k_1 (adsorption constant) values indicate favorable monolayer adsorption of cyclohexanone at the unsaturated active sites. The negative equilibrium (k_{-1}) values suggest re-distribution of free energy in the catalytic systems at equilibrium, while the positive k_2 values (desorption constants) suggest high rates of decomposition and diffusion of AA from an active surface [39]. Also, the

observed $k_2 \gg k_1$ signified monolayer relaxation and reconstruction of the active surface during adsorption, and aggregation of the substrate (cyclohexanone), which has low interference with binding sites; this was further attributed to enhanced (fast) dissociation of adipic acid from the active surface. In addition, the rate of reaction, r (Ms^{-1}), was faster over compound **1** than over compound **2**.

6. Thermodynamic Parameters for the Oxidation of Cyclohexanone

The thermodynamic parameters obtained with compounds **1** and **2** are presented in Table 5. The activation entropy values, ΔS^\ddagger , and the enthalpy of the transition state, ΔH^\ddagger , were determined by using the Arrhenius and Eyring equations [39–41]:

$$\ln \frac{k_1}{T} = -\frac{\Delta H^\ddagger}{R} \cdot \frac{1}{T} + \ln \frac{k_B}{h} + \frac{\Delta S^\ddagger}{R}$$

where k_1 = initial rate constant, k_B = Boltzmann's constant ($1.3 \times 10^{-23} \text{ J.K}^{-1}$), T = temperature in Kelvin, and h = Plank's constant ($6.626 \times 10^{-34} \text{ J.s}$). These values, ΔS^\ddagger and ΔH^\ddagger , are recorded in Tables 3 and 4, and were obtained in a linear plot ($y = mx + c$) of $\ln(k_1/T)$ vs. $1/T$, as shown in Figure S22. The intercept corresponded to $\ln k_B/h + \Delta S^\ddagger/R$; the slope corresponded to $\Delta H^\ddagger/R$. The Gibb's free energy value, ΔG^\ddagger , was obtained from the expression: $\Delta G^\ddagger = \Delta H^\ddagger - T\Delta S^\ddagger$. The activation energy, E_a , was calculated using the expression: $E_a = \Delta H^\ddagger + RT$, where R = universal gas constant ($8.314 \text{ J mol}^{-1} \text{ K}^{-1}$).

Table 5. Thermodynamics parameters for cyclohexanone oxidation over compounds **1** and **2**.

Catalyst	$\Delta G^\ddagger/\text{J mol}^{-1}$	$\Delta S^\ddagger/\text{J mol}^{-1}\text{K}^{-1}$	$\Delta H^\ddagger/\text{KJ mol}^{-1}$	$E_a/\text{J mol}^{-1}$	$t_{1/2}/\text{s}$
1 at 40 °C	−37,256	-	-	-	5,518,763
1 at 80 °C	−43,206	119.0	2.79	3021	-
2 at 40 °C	−38,508	-	-	-	8,781,173
2 at 80 °C	−43,428	122.6	2.81	2938	-

ΔH^\ddagger = activation enthalpy; ΔS^\ddagger = entropy; ΔG^\ddagger = Gibb's free energy; $t_{1/2}$ = half-life of cyclohexanone decomposition.

As shown in Table 5, the ΔG^\ddagger values ($-37,256 \text{ J mol}^{-1}$ and $-38,508 \text{ J mol}^{-1}$) suggest an initial reactivity of non-thermalized molecules at low temperatures [39,41]. However, as the temperature of the catalytic system gradually increased, free energy was distributed, leading to an increase in the negative ΔG^\ddagger values ($-43,206 \text{ J mol}^{-1}$, and $-43,428 \text{ J mol}^{-1}$), via a spontaneous catalytic process. This further indicates that the physisorption condition, under which the adsorption of the cyclohexanone took place on an active surface, became more negative and more favorable by increasing the reaction temperature [40]. The positive entropy, ΔS^\ddagger values (119.0 JK^{-1} , and 122.6 JK^{-1}), suggested that the reacting molecules were liberated from their initial state, to a transition state, due to an increase in the degrees of freedom (ΔS^\ddagger) [39]. Though a transition state was reached which promoted radical reactions, as earlier described in the mechanism of reaction, the radical reactions (of hydroxyl, OH^\bullet , and carboxyl, CyOO^\bullet , groups) led to pre-formation of complex or intermediate products (6-hydroxyhexanoic acid and caprolactone). The Arrhenius and Eyring plots of cyclohexanone oxidation over compounds **1** and **2** are presented in Figure S22. Furthermore, the positive enthalpy, ΔH^\ddagger , values suggest that at optimum temperature, the equilibrium of the catalytic systems moved in the direction that tended to promote complete AA formation [39]. Similarly, as the enthalpies, ΔH^\ddagger , of the adsorbed substrate (2.79 KJ mol^{-1} , and 2.81 KJ mol^{-1}) over compounds **1** and **2**, were less than 40 KJ mol^{-1} , this indicated that physisorption primarily occurred at the coordinatively unsaturated metal (CUM) sites, and that the host-guest interactions involved those of van der Waal's interactions or weak π - π interactions [39]. The partial concave curve (Figure S22) observed for compounds **1** and **2** was attributed to two rate-limiting reaction steps. In addition, the activation energy, E_a value (3021 J mol^{-1}), suggested that compound **1** required more activation energy to catalyze the oxidation of cyclohexanone than compound **2** (2938 J mol^{-1}),

which required less activation energy. The use of acetonitrile as solvent suggested that the access of water into the pore walls of the catalysts was prevented; hence, the reaction rate was enhanced. The TOF of the catalytic reaction with acetonitrile gave 22.9 h^{-1} and 13.9 h^{-1} , respectively.

7. Conclusions

The catalytic activities of Mn(II) and Co(II)-based coordination complexes have been established. Both compounds were considered to be very sensitive to peroxyolytic degradation at specified temperatures ($80 \text{ }^\circ\text{C}$); the hydrolytic stabilities were controlled with Millipore.

Finally, both compounds **1** and **2** exhibited remarkable catalytic activity, with performances better than those of other copper-containing organic frameworks [14,37]. The use of hydrogen peroxide would eliminate the use of nitric acid and the emission of nitrous oxide. Both catalysts are cost-effective, chemically and hydrothermally stable, and can easily be reused after separation from reaction mixture. A lesser amount, $-43,428 \text{ J mol}^{-1}$, of free energy (ΔG^\ddagger) was required by compound **2** to catalyze cyclohexanone oxidation when compared to compound **1**, which required $-43,206 \text{ J mol}^{-1}$. Overall, the rate of reaction was found to be lower ($1.00 \times 10^{-7} \text{ M s}^{-1}$) for compound **2**. Based on the thermodynamic parameters obtained, it was hypothesized that the active surface of the compounds became more unsaturated as chemical reactivity of the surface was taking place, due to monolayer physisorption; these findings are consistent with those reported elsewhere [19].

Supplementary Materials: The following supporting information can be downloaded at: <https://www.mdpi.com/article/10.3390/inorganics10070100/s1>, FTIR spectra of **1** and **2** and their ligands (Figures S1 and S2), UV-Vis. spectra of **1** and **2** and their ligands (Figures S3 and S4), TG Curve of compounds **1** and **2** (Figures S5 and S6), 2D view of compound **1** (010) showing HB interactions between compound **1** and (imi) (Figure S7), 1D view of compound **2** (100) showing network of hydrogen bonds (Figure S8), PXRD patterns (Cu, $K\alpha$) of simulated and crushed samples of compounds **1** and **2** (Figures S9 and S10), High resolution TEM images of **1** and **2** (Figures S11A and S11B), The effect of reaction temperature on the oxidation of cyclohexanone (Figure S12), HPLC chromatogram of an aliquot ($2\mu\text{L}$) taken after oxidation of cyclohexanone in the absence of compound **1** (Figure S13), The effect of catalysts loading on the oxidation of cyclohexanone (Figure S14), The effect of reaction time on the oxidation of cyclohexanone (Mn^{2+} catalyst) (Figures S15A), The effect of reaction time on the oxidation of cyclohexanone (Co^{2+} catalyst) (Figure S15B), HPLC chromatogram of an aliquot of target product with compound **1** as catalyst (Figure S16), UV-Visible spectra studies of reactions (Figure S17), ^1H and ^{13}C NMR spectra (DMSO- D_6) of the isolated adipic acid obtained with compound **1** (Figures S18 and S19), Illustration for the catalytic activities of compounds **1** and **2** (Figure S20), Arrhenius and Eyring plot of cyclohexanone oxidation over compounds **1** and **2** (Figure S21), and L-H plot for the oxidation of cyclohexanone (Figure S22).

Author Contributions: Supervision and funding acquisition, A.C.T. and R.T.; conceptualization, A.Y.I., M.P. and A.T.V.; methodology and writing—original draft, A.Y.I.; formal analysis, M.P. and A.T.V.; writing—review and editing, H.S.C. and A.S.O. All authors have read and agreed to the published version of the manuscript.

Funding: This project was funded by CSIR—TWAS (FR Number: 3240293588).

Institutional Review Board Statement: Not applicable.

Informed Consent Statement: Not applicable.

Data Availability Statement: CCDC 1855628 and 1830759 contain the supplementary crystallographic data for this paper.

Acknowledgments: The authors are grateful to Centre for Scientific and Innovative Research, Delhi; and National Chemical Laboratory, Pune, India for providing facility for the research.

Conflicts of Interest: The authors declare that there is no conflict of interest.

References

1. D'Alessandro, N.; Liberatore, L.; Tonucci, L.; Morvillo, A.; Bressan, M. Direct synthesis of adipic acid by mono-persulfate oxidation of cyclohexane, cyclohexanone or cyclohexanol catalyzed by water-soluble transition-metal complexes. *New J. Chem.* **2001**, *25*, 1319–1324. [[CrossRef](#)]
2. Cavani, F.; Teles, J.H. Sustainability in catalytic oxidation: An alternative approach or a structural evolution? *ChemSusChem* **2009**, *2*, 508–534. [[CrossRef](#)] [[PubMed](#)]
3. Shylesh, S.; Srilakshmi, C.; Singh, A.; Anderson, B. One step synthesis of chromium-containing periodic mesoporous organosilicas and their catalytic activity in the oxidation of cyclohexane. *Microporous Mesoporous Mater.* **2007**, *99*, 334–344. [[CrossRef](#)]
4. Anand, R.; Hamdy, M.; Gkourgkoulas, P.; Maschmeyer, T.; Jansen, J.; Hanefeld, U. Liquid phase oxidation of cyclohexane over transition metal incorporated amorphous 3D-mesoporous silicates M-TUD-1 (M = Ti, Fe, Co and Cr). *Catal. Today* **2006**, *117*, 279–283. [[CrossRef](#)]
5. Gross, A.F.; Sherman, E.; Vajo, J.J. Aqueous room temperature synthesis of cobalt and zinc sodalite zeolitic imidizolate frameworks. *Dalton Trans.* **2012**, *41*, 5458–5460. [[CrossRef](#)] [[PubMed](#)]
6. Hwang, K.C.; Sagadevan, A. One-pot room-temperature conversion of cyclohexane to adipic acid by ozone and UV light. *Science* **2014**, *346*, 1495–1498. [[CrossRef](#)] [[PubMed](#)]
7. Béziat, J.; Besson, M.; Gallezot, P. Liquid phase oxidation of cyclohexanol to adipic acid with molecular oxygen on metal catalysts. *Appl. Catal. A Gen.* **1996**, *135*, L7–L11. [[CrossRef](#)]
8. Van de Vyver, S.; Román-Leshkov, Y. Emerging catalytic processes for the production of adipic acid. *Catal. Sci. Technol.* **2013**, *3*, 1465–1479. [[CrossRef](#)]
9. Benadji, S.; Mazari, T.; Dermeche, L.; Salhi, N.; Cadot, E.; Rabia, C. Clean Alternative for Adipic Acid Synthesis Via Liquid-Phase Oxidation of Cyclohexanone and Cyclohexanol Over H₃–2xCoxPMo₁₂O₄₀ Catalysts with Hydrogen Peroxide. *Catal. Lett.* **2013**, *143*, 749–755. [[CrossRef](#)]
10. Soares, J.C.S.; Gonçalves, A.H.A.; Zotin, F.M.; de Araújo, L.R.R.; Gaspar, A.B. Cyclohexene to adipic acid synthesis using heterogeneous polyoxometalate catalysts. *Mol. Catal.* **2018**, *458*, 223–229. [[CrossRef](#)]
11. Alcañiz-Monge, J.; Trautwein, G.; Garcia-Garcia, A. Influence of peroxometallic intermediaries present on polyoxometalates nanoparticles surface on the adipic acid synthesis. *J. Mol. Catal. A Chem.* **2014**, *394*, 211–216. [[CrossRef](#)]
12. Jianhui, L.; Yichao, H.; Bin, D.; Pingmei, W.; Xiangfei, G.; Jiangwei, Z.; Yongge, W. Single-atom Mn active site in a triol-stabilized β -Anderson manganohexamolybdate for enhanced catalytic activity towards adipic acid production. *Catalysts* **2018**, *8*, 121–134.
13. Oksana, V.N.; Dmytro, S.N.; Agnieszka, K.M.; Fátima, C.G.; Armando, J.L.P. Synthesis, crystal structures and catalytic activity of Cu(II) and Mn(III) schiff base complexes: Influence of additives on the oxidation catalysis of cyclohexane and 1-phenylethanol. *J. Mol. Catal. A Chem.* **2017**, *426*, 506–515.
14. Raja, J.; Ana, P.C.R.; Fátima, C.G.M.; Kamran, T.M.; Maximilian, N.K.; Tatiana, B.A.; Houcine, N.; Gonçalves, A.O.T.; Armando, J.L.P. Polynuclear Copper(II) Complexes as Catalysts for the Peroxidative Oxidation of Cyclohexane in a Room-Temperature Ionic Liquid. *Eur. J. Inorg. Chem.* **2014**, *2014*, 4541–4550.
15. Lien, T.L.N.; Chi, V.N.; Giao, H.D.; Ky, K.A.L.; Nam, T.S.P. Towards applications of metal–organic frameworks in catalysis: Friedel-Crafts acylation reaction over IRMOF-8 as an efficient heterogeneous catalyst. *J. Mol. Catal. A Chem.* **2011**, *349*, 28–35.
16. Chavan, S.; Srinivas, D.; Ratnasamy, P. Oxidation of Cyclohexane, Cyclohexanone, and Cyclohexanol to Adipic Acid by a Non-HNO₃ Route over Co/Mn Cluster Complexes. *J. Catal.* **2002**, *212*, 39–45. [[CrossRef](#)]
17. Maksimchuk, N.; Timofeeva, M.; Mel'Gunov, M.; Shmakov, A.; Chesalov, Y.; Dybtsev, D.; Fedin, V.; Kholdeeva, O. Heterogeneous selective oxidation catalysts based on coordination polymer MIL-101 and transition metal-substituted polyoxometalates. *J. Catal.* **2008**, *257*, 315–323. [[CrossRef](#)]
18. Xamena, F.; Casanova, O.; Tailleux, R.G.; Garcia, H.; Corma, A. Metal organic frameworks (MOFs) as catalysts: A combination of Cu²⁺ and Co²⁺ MOFs as an efficient catalyst for tetralin oxidation. *J. Catal.* **2008**, *255*, 220–227. [[CrossRef](#)]
19. Satoshi, H.; Mircea, D.; Kentaro, T.; Jeffrey, R.L. Size-Selective Lewis Acid Catalysis in a Microporous Metal-Organic Framework with Exposed Mn²⁺ Coordination Sites. *J. Am. Chem. Soc.* **2008**, *130*, 5854–5855.
20. Vandichel, M.; Biswas, S.; Leus, K.; Paier, J.; Sauer, J.; Verstraelen, T.; Van Der Voort, P.; Waroquier, M.; Van Speybroeck, V. Catalytic Performance of Vanadium MIL-47 and Linker-Substituted Variants in the Oxidation of Cyclohexene: A Combined Theoretical and Experimental Approach. *ChemPlusChem* **2014**, *79*, 1183–1197. [[CrossRef](#)]
21. Zhang, H.; Gu, J.; Kirillova, M.V.; Kirillov, A.M. Coordination Polymers Driven by Carboxy Functionalized Picolinate Linkers: Hydrothermal Assembly, Structural Multiplicity, and Catalytic Features. *Cryst. Growth Des.* **2021**, *21*, 5145–5157. [[CrossRef](#)]
22. Pradip, P.; Bikash, G.; Rahul, B. Functionalization and isoreticulation in a series of metal-organic frameworks derived from pyridinecarboxylates. *Inorg. Chem.* **2016**, *55*, 7200–7205.
23. Cravillon, J.; Münzer, S.; Lohmeier, S.-J.; Feldhoff, A.; Huber, K.; Wiebcke, M. Rapid Room-Temperature Synthesis and Characterization of Nanocrystals of a Prototypical Zeolitic Imidazolate Framework. *Chem. Mater.* **2009**, *21*, 1410–1412. [[CrossRef](#)]
24. Tabrizi, L.; Chiniforoshan, H.; McArdle, P. A novel one-dimensional manganese(II) coordination polymer containing both dicyanamide and pyrazinamide ligands: Synthesis, spectroscopic investigations, X-ray studies and evaluation of biological activities. *Spectrochim. Acta Part A Mol. Biomol. Spectrosc.* **2014**, *139*, 307–312. [[CrossRef](#)]
25. Prananto, Y.P. Coordination Polymer of M(II)-Pyrazinamide (M = Co, Cd) with Double End-to-End Thiocyanate Bridge. *IOP Conf. Ser. Mater. Sci. Eng.* **2018**, *299*, 012032. [[CrossRef](#)]

26. Gomez-Lor, B.; Gutierrez-Puebla, E.; Iglesias, M.; Monge, M.A.; Ruiz-Valero, C.; Snejko, N. In(2)(OH)(3)(BDC)(1.5) (BDC = 1,4-benzenedicarboxylate): An In(III) supramolecular 3D framework with catalytic activity. *Inorg. Chem.* **2002**, *41*, 2429. [[CrossRef](#)]
27. Mendoza-Díaz, G.; Rigotti, G.; Piro, O.E.; Sileo, E.E. Solid-state 111Cd NMR studies on cadmium(II)-2,x-pyridinedicarboxylates. Crystal structure of 2,4-pyridinedicarboxylato triaqua cadmium(II) hemihydrate: [Cd(II)(2,4-pydc)(H₂O)₃·1/2H₂O]. *Polyhedron* **2005**, *24*, 777–783. [[CrossRef](#)]
28. Schlichte, K.; Kratzke, T.; Kaskel, S. Improved synthesis, thermal stability and catalytic properties of the metal-organic framework compound Cu₃(BTC)₂. *Microporous Mesoporous Mater.* **2004**, *73*, 81–88. [[CrossRef](#)]
29. Hu, L.; Hao, G.X.; Luo, H.D.; Ke, C.X.; Shi, G.; Lin, J.; Lin, X.M.; Qazi, U.Y.; Cai, Y.P. Bifunctional 2D Cd (II)-based metal-organic framework as efficient heterogeneous catalyst for the formation of C–C bond. *Cryst. Growth Des.* **2018**, *18*, 2883–2889. [[CrossRef](#)]
30. Chauhan, J.S.; Patel, R.P.; Pandya, A.V. Studies of Some Novel Chromium Pyridine Dicarboxylate Complexes. *Orient. J. Chem.* **2014**, *30*, 1763–1769. [[CrossRef](#)]
31. Mohsin, A.; Mansoor, A.; Saleem, H.; Mustafa, K.; Majid, M.; Seyed, A.A. Design, Synthesis and Antitubercular Evaluation of Novel Series of Pyrazinecarboxamide Metal Complexes. *Iran. J. Pharm. Res.* **2016**, *17*, 93–99.
32. Tella, A.C.; Oladipo, A.C.; Adimula, V.O.; Ameen, O.A.; Bourne, S.A.; Ogunlaja, A.S. Synthesis and crystal structures of a copper(ii) dinuclear complex and zinc(ii) coordination polymers as materials for efficient oxidative desulfurization of dibenzothiophene. *New J. Chem.* **2019**, *43*, 14343–14354. [[CrossRef](#)]
33. Loukopoulos, E.; Kostakis, G.E. Review: Recent advances of one-dimensional coordination polymers as catalysts. *J. Coord. Chem.* **2018**, *71*, 371–410. [[CrossRef](#)]
34. Horcajada, P.; Surblé, S.; Serre, C.; Hong, D.-Y.; Seo, Y.-K.; Chang, J.-S.; Grenèche, J.-M.; Margiolaki, I.; Férey, G. Synthesis and catalytic properties of MIL-100(Fe), an iron(iii) carboxylate with large pores. *Chem. Commun.* **2007**, *27*, 2820–2822. [[CrossRef](#)]
35. Da Silva, G.B.; Menezes, P.H.; Malvestiti, I.; Falcão, E.H.; Alves, S., Jr.; Chojnacki, J.; da Silva, F.F. Copper-based 2D-coordination polymer as catalyst for allylation of aldehydes. *J. Mol. Struct.* **2018**, *1155*, 530–535. [[CrossRef](#)]
36. Adam, M.S.S. Catalytic activity of nickel(II), copper(II) and oxovanadium(II)-dihydroindolone complexes towards homogeneous oxidation reactions. *Appl. Organomet. Chem.* **2018**, *32*, e4234. [[CrossRef](#)]
37. Xia, C.; Lin, M.; Zhu, Bin.; Shu, X. Study on the Mechanisms for Baeyer-Villiger Oxidation of Cyclohexanone with Hydrogen Peroxide in Different Systems. *China Pet. Process. Petrochemical Technol.* **2012**, *14*, 7–17.
38. Kumar, K.V.; Porkodi, K.; Rocha, F. Langmuir–Hinshelwood kinetics—A theoretical study. *Catal. Commun.* **2008**, *9*, 82–84. [[CrossRef](#)]
39. Masel, R.I. *Chemical Kinetics and Catalysis*; Wiley-Interscience: New York, NY, USA, 2001; ISBN 0-471-24197-0.
40. Xie, M.-H.; Yang, X.-L.; Wu, C.-D. From 2D to 3D: A Single-Crystal-to-Single-Crystal Photochemical Framework Transformation and Phenylmethanol Oxidation Catalytic Activity. *Chem. A Eur. J.* **2011**, *17*, 11424–11427. [[CrossRef](#)]
41. Jiao, L.; Wang, Y.; Jiang, H.-L.; Xu, Q. Metal-Organic Frameworks as Platforms for Catalytic Applications. *Adv. Mater.* **2017**, *30*, e1703663. [[CrossRef](#)]